JOURNAL OF MATERIALS SCIENCE 18 (1983) 1887–1894

Analysis of layer structure of boronized steel surface by conversion electron Mössbauer spectrometry (CEMS)

ARIMICHI HANDA, YUSUKE UJIHIRA
Faculty of Engineering, University of Tokyo, Hongo 7-3-1, Bunkyo-ku, Tokyo 113, Japan

The surfaces of Cr–Mo–Ni and Cr–Mo steels were boronized by the solid phase reaction with B_4C powders at 900° C for 5 h, and the surfaces of a Cr–Mo steel and a pure iron were boronized by the gas phase reaction in BCl_3 at 800° C for 2 h and reheated at 800° C under vacuum. The layer structures of 4 different samples were studied by applying CEMS to them. The analyses of CEM spectra of exposed surfaces by grinding to the desired depth revealed that the boronized surfaces prepared by the thermal diffusion of boron atoms in the iron lattice at 900° C were, in principle, composed of distinct multi-layers of four iron–boron compounds; FeB_{1+x} ($x > 0$), FeB, Fe_2B and distorted α-Fe. Only the Fe_2B was deposited on the steel surface boronized at 800° C by the gas phase reaction. No intermediate layer between any two compounds was recognized, showing the contrast with the nitrided steel surfaces.

1. Introduction

The surfaces of steel products such as a gear wheel, a cutter and a crankshaft are usually hardened by the boronization, carburization and nitridation processes to prevent defacement or friction. Numbers of papers have been published on the correlations between the crystalline phase and the mechanical properties of the surface layer and the hardening conditions. Only a few papers have dealt with the surface structure of the hardened layer which is one of the most basic points for the surface characteristics.

Recently, St. John and Sammells [1] investigated the uppermost surface layer of boronized steels by X-ray diffractometry (XRD) and have reported that as boronizing time is lengthened from 1 to 5 h the produced compound varies from Fe_2B to FeB via the mixed $Fe_2B + FeB$ phase. The depth resolution of XRD is about 10 μm according to the range of X-ray, so that they reported the results for the surface layer of about 10 μm.

Carbucicchio *et al.* [2] investigated the boronized surface layer of iron, boronized by boron powders at 1000° C for 15 h, by the combinational application of three distinct techniques of Mössbauer spectrometry. The first is conversion electron Mössbauer spectrometry (CEMS), the depth resolution of which is less than 0.1 μm, and the presence of FeB_{1+x} ($x > 0$) and FeB at the top surface was confirmed. The second is X-ray Mössbauer spectrometry (XMS), which has the resolution about 10 μm and showed the existence of FeB and Fe_2B at the 10 μm depth range. The third is transmission Mössbauer spectrometry (TMS) of the detached surface film of iron borides, showing a similar spectrum to the second.

The authors have already published the results of surface layer analyses of the carburized [3], nitrided [4–6], oxidized [7] and phosphated [8–10] steels by means of CEMS. The authors ground the desired thickness of the surface layer which was chemically treated by the appropriate way to harden the surface. In the present study, steels were solid-boronized and gas-boronized under the industrial conditions and then CEM spectra of the exposed layers by grinding was measured. By the repetition of grinding and CEM

0022–2461/83 $03.00 + .12

spectrum observation, layer-by-layer analyses of boronized steel surfaces were achieved.

2. Experimental details

2.1. Sample preparation

Cylindrical specimens (25 mm diameter x 5 mm length) of SCM3 (Cr: 0.9 at %, Mo: 0.3 at %, Ni: 0.4 at %) and S45C (Cr: 1.0 at %, Mo: 0.4 at %) steels were embedded in B_4C powders and boronized by heating the specimens at 900° C for 5 h through a solid phase reaction and cooled to room temperature. The former is nominated sample A and the latter sample B.

A S45C steel and a pure iron were boronized in a gas phase reaction by placing them in BCl_3 gas at 800° C for 2 h, re-heated under vacuum at 800° C for 8 h and annealed (sample C and sample D).

2.2. Observation of cross-sectional views by optical microscope

The samples were cut vertically to the surface and the cross-sectional side of the specimen was polished until mirror-like, etched by nitric acid (5%) and methanol (95%), and the metallographic cross-sectional view was observed with the optical microscope.

2.3. Measurement of the CEM spectrum of the exposed layer

The surfaces of boronized samples were ground mechanically with SiC powders (230–800 mesh) by the desired depth and the CEM spectra of the exposed layers were measured by detecting the re-emitted conversion and Auger electrons by a gas (He 99% + i-C_4H_{10} 1%)-flow proportional counter of 2π geometry manufactured by ourselves or purchased from Austin Science Associates (BSD-2400).

Ortec 459 was used as a high power supply. The output of the detector was passed through a preamplifier (Ortec 142 or 142PC), an amplifier (Ortec 570) and a single channel analyser (Ortec 490B), and connected to a multi-channel analyser (Inotec 5200 or 5300). A γ-source, 20 mCi ^{57}Co(Rh), was fixed to a vibrator (Austin K-3) driven in a constant acceleration mode by a wave function generator (Austin S-600). Mössbauer spectra were computer fitted with the restriction that all peaks had Lorentzian shapes.

3. Results and discussion

3.1. Layer structure of boronized steel produced by the solid-phase reaction with B_4C powders

We could not recognize any difference in the structure of the compound layers between boronized SCM3 (sample A) and S45C (sample B) steels.

Four distinct layers were seen in the metallograph of the boronized SCM3 steel surface (Fig. 1). The uppermost layer was about 80 μm thick and with a needle-like phase. The second layer (80 to about 140 μm), seen as black, was thin. The third was 200 μm thick and composed of a minute crystalline phase. The deepest layer was composed of polycrystalline α-Fe with large grains.

A CEM spectrum of each exposed layer is

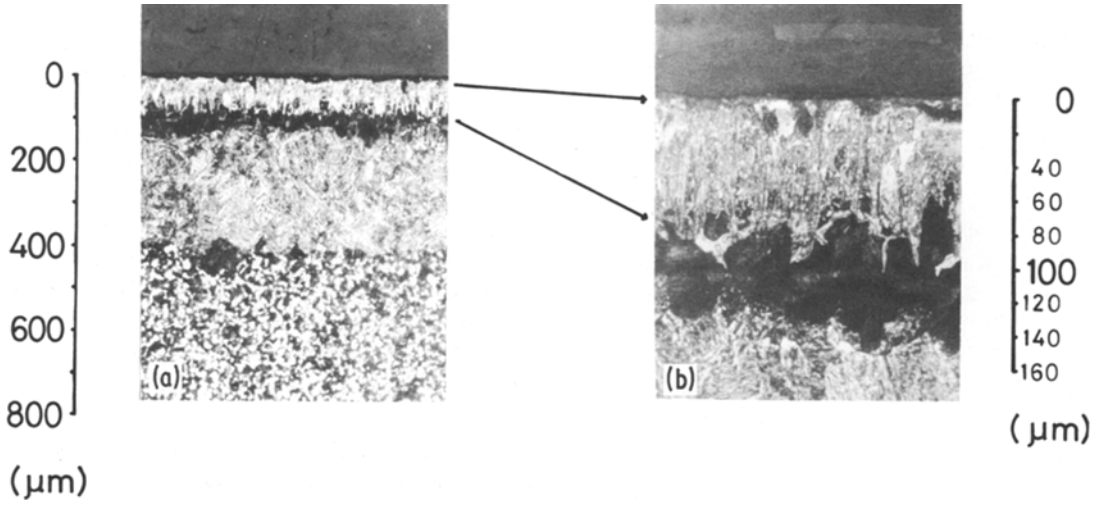

Figure 1 The metallographic cross-section of a SCM3 steel boronized by solid phase reaction with B_4C, Sample A. A: × 100, B: × 400.

shown in Fig. 2. The surface layer is attributed to FeB by XRD. However, CEM spectrum of the top surface is as complicated as 2A and cannot be clearly resolved into discrete components. The internal magnetic field of the phase is smaller than that of FeB. As it is known that the increase of boron content in iron–boron compounds results in the decrease in the strength of the internal magnetic field [11], the uppermost layer can be attributed to FeB_{1+x} ($x > 0$).

The spectrum of the 5 μm depth layer is shown as 2B in Fig. 2. The magnitude of the internal magnetic field corresponds to that of FeB [11–13]. The presence of FeB in the boronized steel surface is also supported by the X-ray diffraction pattern of the surface.

From the comparison of the two simulated spectra, synthesized by a least-squares fit programme assuming either a single sextet or two sextet peaks, it is concluded that the CEM spectrum of 2B has obviously two or more components. Mössbauer parameters derived from two sextet peaks (X and Y) are shown in Table I.

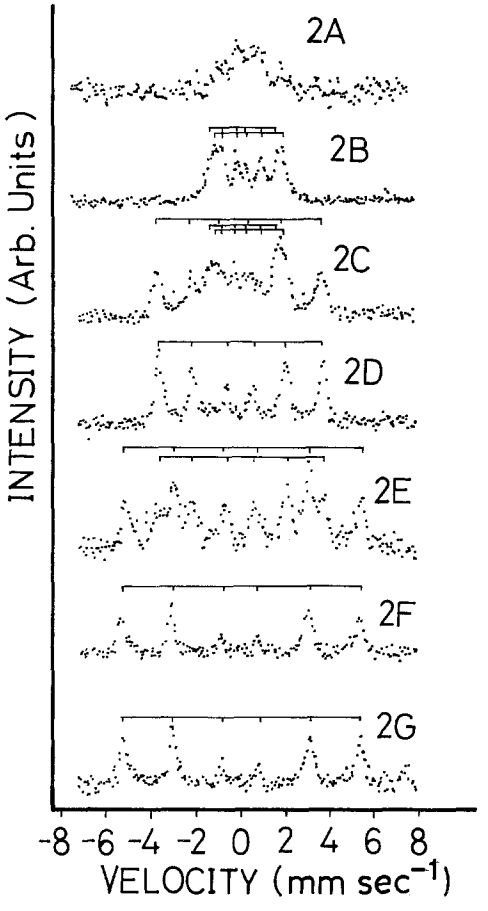

Figure 2 CEM spectra of compound layers of a SCM3 steel boronized by solid phase reaction with B_4C, Sample A. 2A: uppermost surface, 2B: 5 μm, 2C: 20 μm, 2D: 33 μm, 2E: 89 μm, 2F: 130 μm, 2G: a SMC3 steel.

One interpretation of 2B is to assign both sextet peaks to FeB, assuming that two iron sites in a unit cell of FeB. Another interpretation is to treat the spectrum as the superposition of the two different peaks due to different iron borides. Because only FeB was confirmed in the X-ray diffraction pattern at the top surface, we would adopt the former interpretation, which was supported by the results of analysis of the CEM spectrum of the next deeper layer.

The spectrum of the 33 μm depth layer is shown as 2C. It is composed of the superposed spectra of FeB and Fe_2B. If X and Y are different compounds each one located at a different depth layer, 2C may have either X or Y because the layer giving 2C lies beneath the layer of 2B. Since the difference of the profile between 2B and 2C (FeB + Fe_2B) coincides with 2D (Fe_2B), it is concluded that both X and Y of 2B belong to FeB.

Although the FeB crystal has an orthorhombic structure and iron atoms in a unit cell are crystallographically equivalent [14], the two sites of different chemical environment can be caused by the combined interaction between a magnetic field and an electric field gradient (EFG) to the nucleus. Timoshchuk and Vlasov [15] reported that FeB is ferromagnetic and that the axis of easy magnetization is [0 1 0]. But the direction of the principal axis of EFG is different due to the distinct geometrical location of boron. The eigenvalue of energy is expressed as

$$E = -g_N\beta_N H_{int} m + [(-1)^{m+1} e^2 q Q(3\cos^2\theta - 1)]/8$$

where g_N is the nuclear g factor, β_N is the nuclear magneton, H_{int} is the internal magnetic field at the iron nucleus, m is the z component of nuclear spin quantum number, eq is the z component of electric field gradient, eQ is the nuclear quadrupole moment and where θ is the angle between the EFG tensor and the magnetic moment and the θ's for X and Y are different. The H_{int}'s of X and Y are in accordance with each other within experimental error.

The cause of the existence of X and Y can be also explained by the coordination of boron atoms to iron atoms. Although several reports were published on the crystal structure of FeB, we cannot

TABLE I The Mössbauer parameters of iron borides

FeB	H_{int}	IS	QS	Fe_2B	H_{int}	IS	QS	Fe_3B	H_{int}	IS	QS	α-Fe	H_{int}	IS	LW
[11]	11.8	0.28	0.0	[11]	24.2	0.16	–	[20]	23.5	0.07	0.024	*A			
[12]	11.8	0.4	–	[12]	24.2	0.4	–		26.4	0.013	0.11	106 μm	33.9	0.0	0.74
[13]	12.96	0.263	0.061	[17]	24.2	0.17	0.05		28.7	0.08	–	130 μm	33.4	0.0	0.70
*A	9.74	0.26	0.05		23.2	0.17	0.01	[21]	22.5	0.12	–	160 μm	33.0	0.0	0.47
	9.5	0.10	0.36	[18]	24.20	0.119	0.036		26.7	0.04	–	SCM3	33.0	0.0	0.41
*B	10.18	–	0.12		23.17	0.121	0.021					*C			
	9.7	–	0.27	*A								30 μm	32.8	0.06	0.33
*D	9.5	–	–	33 μm	23.1	0.086	–					70 μm	33.0	0.06	0.30
	9.3	–	–	50 μm	23.1	0.088	–					100 μm	33.0	0.03	0.31
				66 μm	23.1	–	–								
				*C											
				8 μm	23.0	–	–								
				18 μm	23.1	–	–								

H_{int}: internal magnetic field (tesla).
IS: isomer shift (mm sec^{-1}).
QS: quadrupole splitting (mm sec^{-1}).
LW: line width (mm sec^{-1}).
*: obtained results in this investigation.
(experimental error; ± 0.07 mm sec^{-1} or ± 0.3 T)

obtain definite data of it. The authors calculated the distances between iron and boron in FeB bondage based on Wycoff's data [14]. Four iron atoms in a unit cell was distinguished into two classes according to the Fe–B distances. Two iron atoms of X are either coordinated with a boron atom apart from the iron atom by 0.211 nm or with two boron atoms by 0.213 nm. The other two iron atoms in Y are coordinated with one and two boron atoms by the distances of 0.211 and 0.219 nm. If Wycoff's data is precise and the EFG is influenced by the coordination of boron atoms, the Mössbauer spectrum can be composed of two different spectra.

This was a report that proposed the probable presence of two crystal types of FeB, α and β, which would be similar to each other from the view point of the Mössbauer spectrum, X-ray diffraction pattern and magnetic property [16]. Owing to this explanation, 2B is considered to be composed of the spectra due to α and β types of FeB.

CEM spectra of FeB for samples B and D can be divided into two components. The slight difference of the profile among samples A, B and D can be explained by the variations in the ratio of iron and boron and the degree of distortion of the crystal structure from those of genuine FeB (Table I).

The spectra of 48 μm depth layer (2D) and 66 μm depth layer are attributed to Fe_2B. The broad FWHM and asymmetry of a sextet peak are caused by the superposition of several spectra due to the various iron atoms which locate distinct sites in Fe_2B [11, 12, 17, 18]. The peak area ratio of the magnetically split peaks of Fe_2B is approximately 3:2:1:1:2:3, indicating random orientation of the magnetic moments of iron atoms.

The layer apart from the uppermost surface by 90 μm is attributed to the mixture of Fe_2B and distorted α-Fe (2E). Although metallographical observation (Fig. 1) indicated the existence of a black and thin layer between Fe_2B and the distorted α-Fe layers, the CEM spectra denied the presence of any particular phase corresponding to the black layer observed in the metallography. This phase could be eutectic phase of α-Fe and Fe_2B [19]. It was reported that Fe_3B [20, 21] was formed during the crystallization of amorphous alloys of iron and boron [22, 23] but metastable Fe_3B cannot be detected in the boronized steel surfaces.

CEM spectra revealed that the materials of the layers apart from the uppermost surface by 110, 130 and 160 μm (2F) are due to the distorted α-Fe, which results by the intrusion of boron atoms into the lattice of α-Fe. Though H_{int}'s and *Q.S.* (quadrupole splitting) coincide with those of α-Fe within the experimental eror, FWHM's of individual peaks and magnitudes of H_{int}'s approach to those of α-iron along with depth (Table I). This evidence indicates the variation of the soluted boron content with depth.

3.2. Layer structure of steel surface boronized by gas reaction in BCl_3 atmosphere

Fig. 3 illustrates the cross-sectional views of gas boronized S45C steel. A black, thin layer of a thick minute layer is not seen in Fig. 3.

By the analyses of CEM spectra of gas-boronized S45C steel, the uppermost surface was attributed to Fe_2B. The mixture of Fe_2B and α-Fe was observed for 30 to 70 μm depth and beneath 70 μm was the layer of α-Fe. The Mössbauer parameters of α-iron did not show any variation along with the distance from the uppermost surface (Table I).

Fig. 4 shows the cross-sectional views of the gas-boronized α-iron. A needle-like layer is seen in the photograph, but a singular layer between the needle-like layer and the metal layer of big grains does not exist.

The outward appearance of the uppermost surface of gas-boronized α-iron was grey similar to those of boronized steels by solid-phase or gas-phase reaction. Any singular appearance could not be recognized for the gas-boronized α-iron. Nevertheless a CEM spectrum of the uppermost surface could not be observed for the gas-boronized α-iron. Insulated materials or low iron content iron boride might have been produced on the uppermost surface.

The layer from the top surface by 2.5 μm was composed of FeB. The mixture of FeB and Fe_2B constitutes the 30 μm depth layer. Beneath 50 μm depth layer were Fe_2B and α-Fe. The layer of α-Fe appeared beneath 70 μm.

4. Conclusions

The thickness measured by CEMS is about 100 nm and thinner than that observed by X-ray diffractometry (about 10 μm), so that the application of CEMS to the exposed solid surface after grinding to the desired depth can afford the information of the more precise layer structures.

The present CEMS study of the boronized

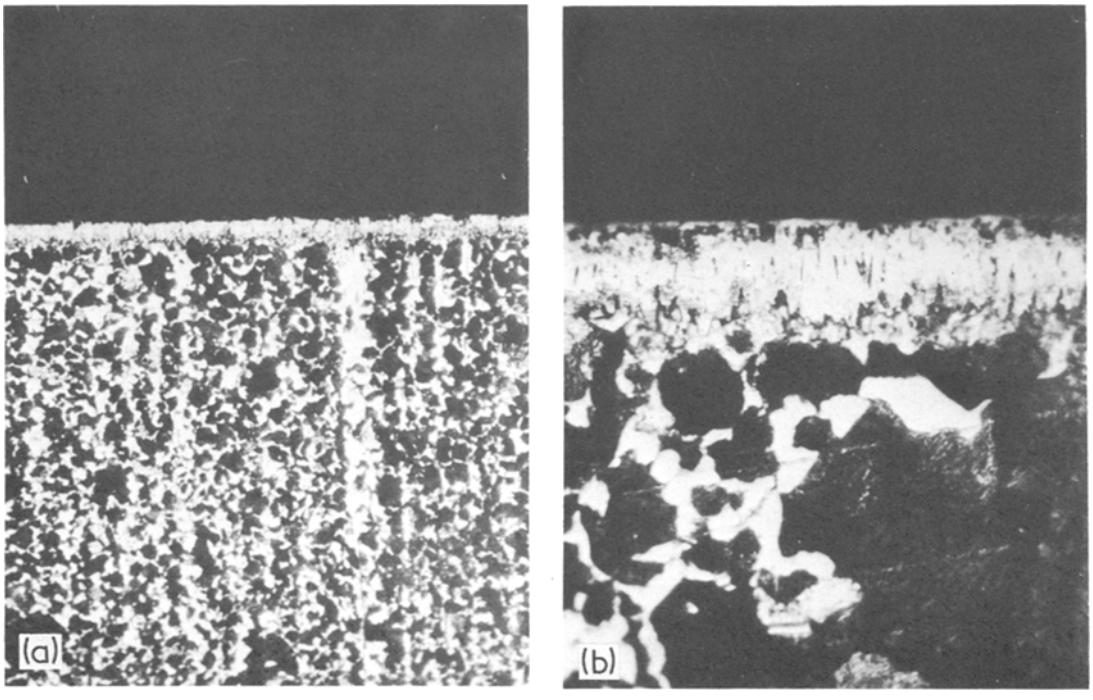

Figure 3 The metallographic cross-section of a S45C steel boronized by gas phase reaction in BCl_3, Sample C. (a) × 100, (b) × 400.

steels gives information about the chemical state of the iron of the boronized surface layer.

1. There exists FeB_{1+x} $(x > 0)$ layer thinner than 5 μm on the steel boronized by solid-phase reaction with B_4C.

2. Crystallographically equivalent iron atoms in a unit cell are divided into two species. Furthermore, Mössbauer parameters of FeB's produced in the boronized steels show a slight difference from one another, indicating that FeB in the boronized layer is distorted to various extents from the pure FeB.

3. Fe_2B layers do not show any difference in Mössbauer parameters among each other due to the sample preparation method or the depth where it exists.

4. The black and thin layer observed in the metallograph of a steel boronized by solid reaction is attributed to the mixture of Fe_2B and α-Fe. The thick and minute layer is attributed to α-Fe in which boron atoms intruded.

5. The Mössbauer parameters of α-Fe of the boronized steel by the solid-phase reaction show the difference due to the depth indicating the decrease of the boron to iron ratio with the distance from the top surface. The Mössbauer parameters of α-Fe in the gas-boronized S45C steel do not show any difference along the depth. The fact is explained by the diffusion of boron atoms to the deeper layer during the re-heating after gas-boronization, so that the distortion of the α-Fe lattice by the intrusion of boron is slight.

6. The structure of boronized steel layer by the thermal treatment with B_4C powders is concluded as follows;

$$\underset{\text{(depth)}}{FeB_{1+x}\ (x>0)}/\underset{(5\,\mu m)}{\text{distorted } \eta\text{-FeB}}/\underset{(30\sim 50\,\mu m)}{\eta\text{-FeB} + \epsilon\text{-}Fe_2B}/$$

$$\underset{(90\sim 110\,\mu m)}{\epsilon\text{-}Fe_2B}/\underset{(110\,\mu m\sim)}{\epsilon\text{-}Fe_2B + \alpha\text{-Fe}}/\text{distorted } \alpha\text{-Fe.}$$

$$\underset{(50\sim 90\,\mu m)}{\text{homogeneous}}$$

The results are different from what was expected on the basis of a thermodynamic view [24].

It was supposed that the chemical potential of boron atoms should gradually decrease inward from the surface with the heating time and that a certain compound should be produced at a local point in an iron boride layer in accordance with the chemical potential of boron atoms at the point. The ΔG–T diagram of Fe–B system has not been reported because of the lack of sufficient

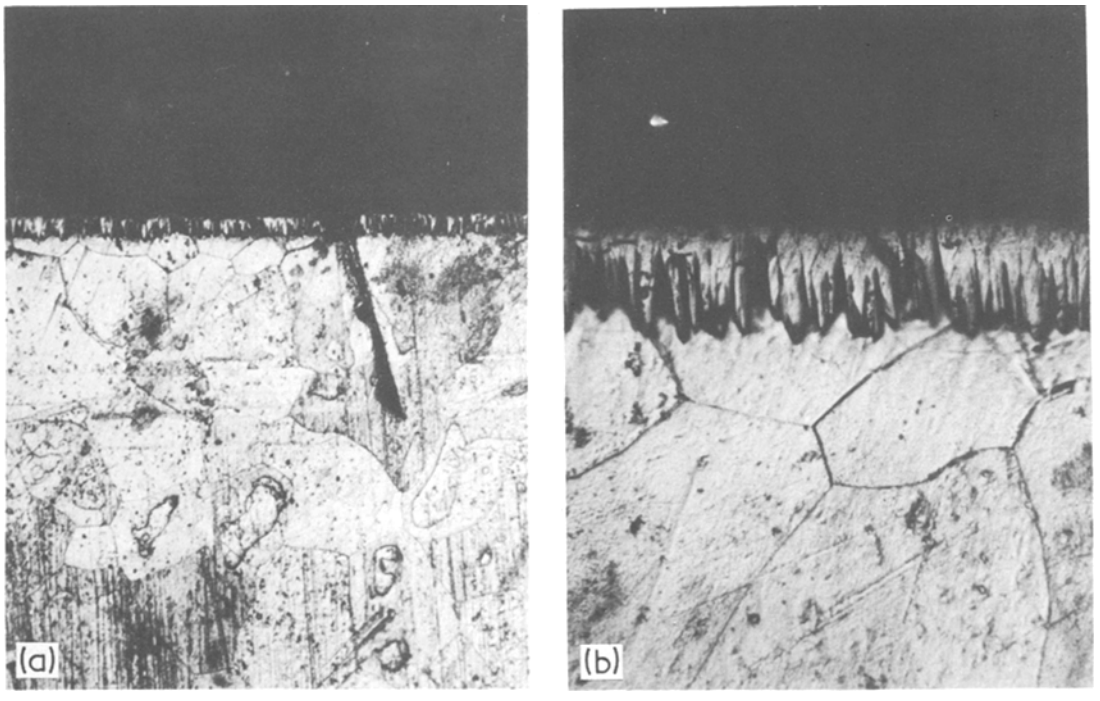

Figure 4 The metallographic cross-section of a α-iron boronized by gas phase reaction in BCl_3, Sample D. A: × 100, B: × 400.

thermodynamic data. It was regarded that the direction of the decrease of boron-potential should correspond to the direction of decrease of boron concentration in the composition–temperature diagram of the system, so that the structure of the iron boride layer might be expected to some extent. Based on the above assumptions, η-FeB, ϵ-Fe_2B and α-Fe, in this order, were expected to form at the surface layer. The results of analyses roughly agree with the presumption. However, some unexpected points also appeared in the prepared samples as follows,

(i) the appearance of FeB_{1+x} $(x > 0)$,

(ii) the decrease of the distortion of α-iron phase along the depth of the phase,

(iii) the homogeneity of Fe_2B phase, and

(iv) the appearance of mixed layer: η-phase + ϵ-phase and ϵ-phase + α-phase.

One of the reasons why the above points could not be expected is the lack of enough and precise $\Delta G-T$ diagram of Fe–B system. Concerning (i) and (iv), it is pointed out that there is one more reason that in the previous assumptions, the iron boride layer produced during the boronization process through the static way. In fact the boronization proceeds by the dynamic way.

Previously authors reported that in the case of the nitrided layer [4–6] the variation in the ratio of iron to nitrogen at a nitrided surface was smooth from 2 to 4 along the depth. On the other hand, the ratio of iron to boron of the boronized layer is discrete. It can be mentioned that the formation of non-stoichiometric compounds of iron and boron are less favourable than those between iron and nitrogen.

Acknowledgements

We thank Drs T. Katagiri and K. Fujii, Faculty of Engineering, Tokyo Metropolitan University and Mr R. Kawada, Parker Thermal Treatment Industry Co. Ltd. for their kindness in the preparation of the boronized steels.

References

1. M. R. ST. JOHN and A. F. SAMMELLS, *J. Mater. Sci.* **16** (1981) 2327.
2. M. CARBUCICCHIO, L. BARDANI and G. PALOMBARINI, *ibid.* **15** (1980) 711.
3. A. HANDA, I. OKABE and Y. UJIHIRA, *ibid.* **16** (1981) 1999.
4. Y. UJIHIRA and A. HANDA, *J. Phys.* **C40** (1979) 586.
5. Y. UJIHIRA, A. HANDA, Y. ABE and I. OKABE, *Nippon Kagakukaishi* **1979** (1979) 234.
6. M. INABA, H. NAKAGAWA and Y. UJIHIRA, *J. Mater. Sci.* **16** (1981) 1712.

7. Y. UJIHIRA and K. NOMURA, *Bunseki Kagaku* **43** (1981) 782.
8. K. NOMURA, Y. UJIHIRA, Y. MATSUSHIMA, R. KOJIMA and Y. SUGAWARA, *Nippon Kagakukaishi* **1980** (1980) 1372.
9. K. NOMURA and Y. UJIHIRA, *J. Mater. Sci.* in press.
10. K. NOMURA and Y. UJIHIRA, *Nippon Kagakukaishi* **1982** (1982) 1352.
11. J. D. COOPER, T. C. GIBB, N. N. GREENWOOD and R. V. PARISH, *Trans. Faraday Soc.* **60** (1964) 2097.
12. T. SHINJO, F. ITOH, H. TAKAKI, Y. NAKAMURA and N. SHIKAZONO, *J. Phys. Soc. Jpn.* **19** (1964) 1252.
13. T. NAKUMURA and S. SHIMIZU, *Bull. Inst. Chem. Res. Kyoto Univ.* **42** (1964) 299.
14. R. W. G. WYCOFF, "Crystal Structures" Vol. 1 (Interscience Publishers, New York, 1960) Chap. 3, p. 56.
15. V. I. TIMOSHCHUK and K. B. VLASOV, *Fiz. Tverd. Tela (Leningrad)* **23** (1981) 931.
16. T. KANAIZUKA, *Phys. Status Solidi A* **69** (1982) 739.
17. I. D. WEISSMAN, L. J. SWARTZENDRUBER and L. H. BENNETT, *Phys. Rev.* **177** (1969) 465.
18. L. TAKACS, M. C. CADEVILLE and I. VENCZE, *J. Phys. F* **5** (1975) 800.
19. T. KATAGIRI, F. FUJII and T. SAGA, *Met. Eng.* **29** (1978) 256.
20. W. K. CHOO and R. KAPLOW, *Met. Trans. A* **8** (1977) 417.
21. G. LeCAER and J. M. DUBOIS, *Phys. Status Solidi A* **64** (1982) 275.
22. R. OSHIMA and F. E. FUJITA, *Jpn. J. Appl. Phys.* **20** (1981) 1.
23. B. BHANU, A. K. BHATNAGAR and R. JAGANNATHAN, *Solid State Commun.* **36** (1980) 661.
24. K. FUEKI, *Nippon Kinzoku Gakkai Kaiho* **14** (1975) 125.

Received 25 October
and accepted 23 November 1982